

# UC Santa Barbara

## UC Santa Barbara Previously Published Works

### Title

ErAs : InGaAs/InGaAlAs superlattice thin-film power generator array

### Permalink

<https://escholarship.org/uc/item/4vq8n11q>

### Journal

Applied Physics Letters, 88(11)

### ISSN

0003-6951

### Authors

Zeng, G H  
Bowers, J E  
Zide, JMO  
et al.

### Publication Date

2006-03-01

Peer reviewed

## ErAs:InGaAs/InGaAlAs superlattice thin-film power generator array

Gehong Zeng<sup>a)</sup> and John E. Bowers

*Department of Electrical and Computer Engineering, University of California, Santa Barbara, California 93106*

Joshua M. O. Zide and Arthur C. Gossard

*Materials Department, University of California, Santa Barbara, California 93106*

Woochul Kim, Suzanne Singer, and Arun Majumdar

*Department of Mechanical Engineering, University of California, Berkeley, California 94720*

Rajeev Singh, Zhixi Bian, Yan Zhang, and Ali Shakouri

*Electrical Engineering Department, University of California, Santa Cruz, California 95064*

(Received 29 August 2005; accepted 13 February 2006; published online 14 March 2006)

We report a wafer scale approach for the fabrication of thin-film power generators composed of arrays of 400 *p* and *n* type ErAs:InGaAs/InGaAlAs superlattice thermoelectric elements. The elements incorporate ErAs metallic nanoparticles into the semiconductor superlattice structure to provide charge carriers and create scattering centers for phonons. *p*- and *n*-type ErAs:InGaAs/InGaAlAs superlattices with a total thickness of 5  $\mu\text{m}$  were grown on InP substrate using molecular beam epitaxy. The cross-plane Seebeck coefficients and cross-plane thermal conductivity of the superlattice were measured using test pattern devices and the  $3\omega$  method, respectively. Four hundred element power generators were fabricated from these 5  $\mu\text{m}$  thick, 200  $\mu\text{m} \times 200 \mu\text{m}$  in area superlattice elements. The output power was over 0.7 mW for an external resistor of 100  $\Omega$  with a 30 K temperature difference drop across the generator. We discuss the limitations to the generator performance and provide suggestions for improvements. © 2006 American Institute of Physics. [DOI: 10.1063/1.2186387]

A number of approaches are being pursued to improve the performance of solid state power generators.<sup>1–5</sup> The performance of thermoelectric devices is largely dependent on the material figure-of-merit  $Z = \frac{\alpha^2 \sigma}{\kappa}$ , where  $\alpha$  is the material Seebeck coefficient,  $\sigma$  is the electrical conductivity, and  $\kappa$  is the thermal conductivity. A large figure-of-merit  $Z$  is necessary for high power densities and high efficiency. A lot of research has been done to improve material thermoelectric properties over bulk or alloy using superlattice structures.<sup>6–12</sup> Heterostructures can enhance thermoelectrical device performance by the selective emission of hot carriers above the barrier layer through thermionic emissions.<sup>13</sup> Interfaces between materials become significantly important on small length scales. Low dimensional structures could overcome the efficiency barriers imposed by the physical limit of conventional bulk materials.<sup>14–17</sup> Superlattice interfaces provides phonon scattering centers to reduce the cross-plane thermal conductivity.<sup>18</sup> To achieve high thermoelectric conversion efficiency,<sup>19</sup> we suggested using nonplanar barriers and embedded quantum dot structures. The incorporation of erbium arsenide metallic nanoparticles into the InGaAs/InGaAlAs superlattice can provide both charge carriers and create scattering centers for phonons. In this letter, we report the fabrication and characterization of 400 element thin-film array power generators using these ErAs:InGaAs/InGaAlAs superlattices.

ErAs:InGaAs/InGaAlAs superlattice samples were grown on (100) InP substrates using a Varian Gen II molecular beam epitaxy (MBE) system.<sup>20</sup> Erbium particles are randomly distributed through the InGaAs layers, which

provide  $2 \times 10^{18} \text{ cm}^{-3}$  doping. Silicon co-doping was used for the *n*-ErAs:InGaAs/InGaAlAs sample; the *p*-ErAs:InGaAs/InGaAlAs sample was co-doped with Be. The 5  $\mu\text{m}$  thick superlattice structure consists of 70 periods of 10 nm InGaAlAs and 20 nm InGaAs, and the 10 nm InGaAlAs layer consists of a digital alloy of 60% InGaAs and 40% InAlAs. 0.3% ErAs is randomly distributed in the 20 nm InGaAs layer.

Cross-plane and in-plane Seebeck coefficients of a superlattice are usually different due to the electron filtering effects of superlattice heterostructure. Two sets of eight 2.1  $\mu\text{m}$  thick *n*-ErAs:InGaAs/InGaAlAs superlattice samples were systematically grown on conductive and insulating InP substrates using MBE with effective doping of  $2 \times 10^{18}$ ,  $4 \times 10^{18}$ ,  $6 \times 10^{18}$ , and  $1 \times 10^{19} \text{ cm}^{-3}$ , respectively. The in-plane Seebeck coefficients of 183, 120, 100, and 70  $\mu\text{V/K}$  were measured for the first set of four samples grown on insulating InP substrates with effective doping of  $2 \times 10^{18}$ ,  $4 \times 10^{18}$ ,  $6 \times 10^{18}$ , and  $1 \times 10^{19} \text{ cm}^{-3}$ , respectively. In order to measure the cross-plane Seebeck coefficients for the second set of the other four samples grown on conductive InP substrates, test pattern devices were fabricated on these four samples. Mesas 5  $\mu\text{m}$  high were formed by reactive ion etching. Microheaters of Ti/Au wire were formed on top of these mesas and used for a local temperature buildup. The microheater metal wires and contact metal layer were insulated with a 300 nm thick layer of  $\text{Si}_3\text{N}_4$ . The device structure is shown in Fig. 1. The temperature difference  $\Delta T$  versus output voltage  $V$  are simultaneously measured, and the data linear fitting value  $\alpha_{\text{com}} = V/\Delta T$  is a combined Seebeck coefficient, which contributes from both the InP substrate and the cross-plane superlattice, and is expressed as:  $\alpha_{\text{com}}$

<sup>a)</sup>Electronic mail: gehong@ece.ucsb.edu

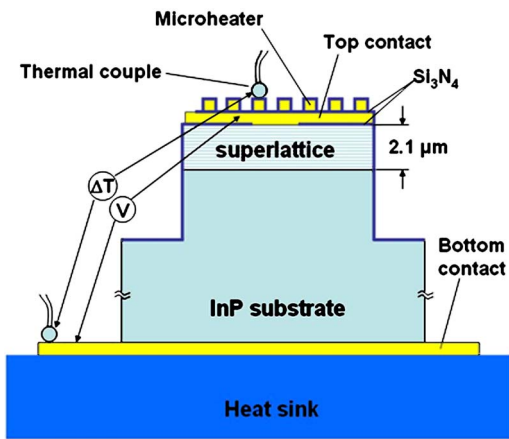


FIG. 1. (Color online) Schematic diagram of a test pattern device for the cross-plane Seebeck coefficient measurement. The superlattice structure is 2.1  $\mu\text{m}$  thick, and the mesa formed by reactive ion etching is about 5  $\mu\text{m}$  high.

$=\alpha_{\text{SL}} \cdot \Delta T_{\text{SL}} / \Delta T + \alpha_{\text{InP}} \cdot \Delta T_{\text{InP}} / \Delta T$  [Eq. (1)], where  $\Delta T$  is the total temperature drop,  $\Delta T_{\text{SL}}$  and  $\Delta T_{\text{InP}}$  are the temperature drop across superlattice and InP substrate, respectively,  $\Delta T = \Delta T_{\text{SL}} + \Delta T_{\text{InP}}$ ;  $\alpha_{\text{SL}}$  is cross-plane Seebeck coefficient of the superlattice, and  $\alpha_{\text{InP}}$  is Seebeck coefficient of the InP substrate.  $\alpha_{\text{InP}}$  can be obtained using direct bulk Seebeck coefficient measurements, and  $\Delta T_{\text{SL}} / \Delta T_{\text{InP}}$  can be determined via (3D) finite element modeling.<sup>21</sup> Room temperature cross-plane Seebeck coefficients of 509, 422, 341, and 290  $\mu\text{V}/\text{K}$  were measured for the four  $n$ -ErAs:InGaAs/InGaAlAs superlattice samples with the effective doping of  $2 \times 10^{18}$ ,  $4 \times 10^{18}$ ,  $6 \times 10^{18}$ , and  $1 \times 10^{19} \text{ cm}^{-3}$ , respectively. The improvements in the cross-plane Seebeck coefficients over the in-plane Seebeck coefficients are due to the electron filtering effects of superlattice heterostructure barriers.

The thermal conductivity is also a key factor for achieving good performance of a power generator. The cross-plane thermal conductivity of ErAs:InGaAs/InGaAlAs superlattices with different erbium concentrations was measured using the  $3\omega$  method.<sup>22</sup> The measurement results in Fig. 2 show that the phonon scattering produced by the superlattice

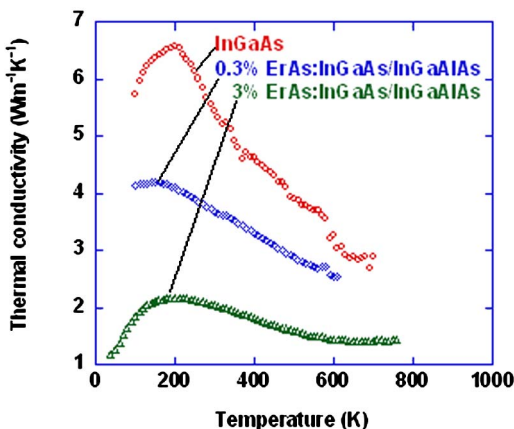


FIG. 2. (Color online) The thermal conductivity of an InGaAs alloy sample, and the cross-plane thermal conductivity of a 0.3% ErAs:InGaAs/InGaAlAs superlattice sample and a 3% ErAs:InGaAs/InGaAlAs superlattice sample were measured, respectively. The results show the phonon scattering produced by the superlattice heterostructure interface and the ErAs nanoparticles is a key factor in the thermal conductivity reduction.

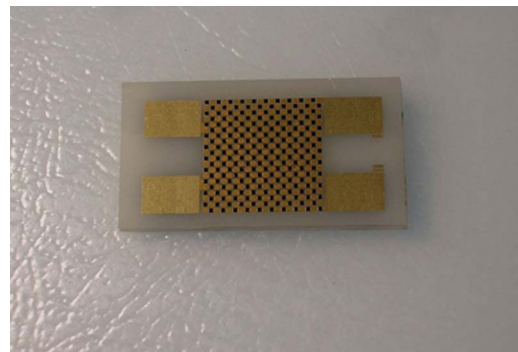


FIG. 3. (Color online) A 200  $n$ -ErAs:InGaAs/InGaAlAs superlattice element array was bonded on a lower AlN plate 650  $\mu\text{m}$  thick. The superlattice element is 5  $\mu\text{m}$  thick and 200  $\mu\text{m} \times 200 \mu\text{m}$  in area size.

heterostructure interface and ErAs nanoparticles played an important role in the thermal conductivity reduction.

The processing of ErAs:InGaAs/InGaAlAs superlattice element array is compatible with an integrated circuit fabrication process. Mesas 7  $\mu\text{m}$  high and 200  $\mu\text{m} \times 200 \mu\text{m}$  in area size were formed by dry etching into the InP substrate, and contact and bonding metal layers were deposited on top of these elements using electron beam evaporation. Ni/GeAu metallization was used for ohmic contact to the superlattice elements, and  $n$ -type specific contact resistivity on the order of  $10^{-7} \Omega \text{ cm}^2$  was measured from room temperature up to 250  $^{\circ}\text{C}$ . The array generator was formed via flip-chip bonding: A 200 element  $n$ -ErAs:InGaAs/InGaAlAs array and a 200 element  $p$ -ErAs:InGaAs/InGaAlAs array were bonded to 650  $\mu\text{m}$  thick lower and upper AlN plates, respectively. The InP substrates were removed by wet etching to form  $n$  and  $p$  thin-film element array. Figure 3 shows a 200  $n$ -ErAs:InGaAs/InGaAlAs superlattice element array bonded on a lower AlN plate. Finally, the 400 element thin-film array generator, shown in Fig. 4, was formed by flip-chip bonding of the 200  $n$ -type element array on a lower AlN plate and the 200  $p$ -type element array on an upper AlN plate together. The dependence of output power on temperature difference across the generator and different electrical loads is shown in Fig. 5. Over 0.7 mW output power was measured on an external load resistor of 100  $\Omega$ .

The output power can be expressed as

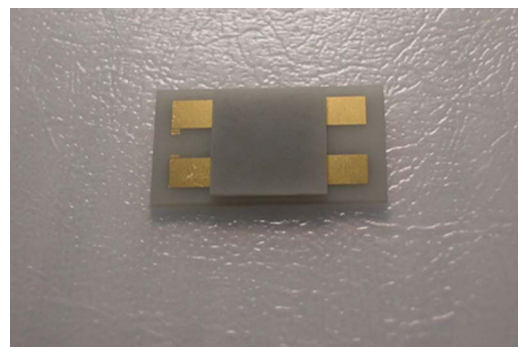


FIG. 4. (Color online) A 400 element ErAs:InGaAs/InGaAlAs superlattice power generator, which was formed by flip-chip bonding of the 200  $n$ -type superlattice elements on a lower AlN plate and the 200  $p$ -type superlattice elements on an upper AlN plate together. The element is 5  $\mu\text{m}$  thick and 200  $\mu\text{m} \times 200 \mu\text{m}$  in area size, and the upper and lower AlN plates are 650  $\mu\text{m}$  thick each.

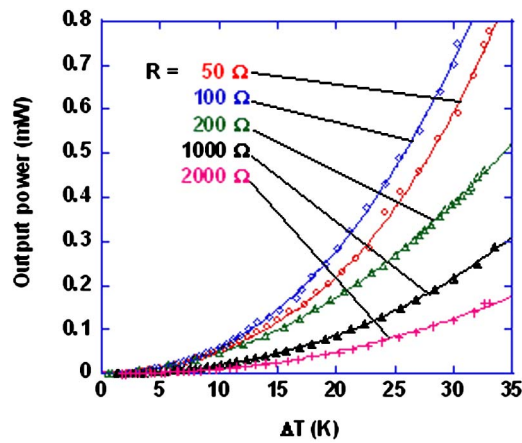


FIG. 5. (Color online) The measurement results of the output power on an external load resistor  $R$  with the temperature difference drop across the generator up to 33 K and the external resistance ranging from 50 to 2000  $\Omega$ .

$$P = R \left( \frac{\alpha \cdot \Delta T_e}{R + r} \right)^2,$$

where  $\Delta T_e$  is the temperature drop across the superlattice thin film elements,  $\alpha$  is the Seebeck coefficient,  $R$  is the external electrical load resistance, and  $r$  is the internal resistance of the module. Thermal simulations show that 85% of the temperature drop was across the two 650  $\mu\text{m}$  thick AlN plates while only about 15% of the temperature drop was across the 5  $\mu\text{m}$  thick ErAs:InGaAs/InGaAlAs superlattice array elements. Such a small temperature drop ratio on the array element is a major limitation to the generator's performance. This can be greatly improved by using thinner AlN plates or by using a higher thermal conductivity material, such as diamond, for the package plates. It can also be improved by increasing the superlattice element thickness. The internal parasitic resistance loss, which includes resistance of internal metal connections and the contact resistance, is another limitation. Because the thin film superlattice elements are only 5  $\mu\text{m}$  thick, the resistance of each thin-film element is at most only a few milliohms, which makes the contact resistance a dominant factor. Reducing the contact resistance and the resistance of the internal connections is needed.

Fundamentally, the generator performance is determined by the thermoelectric  $ZT$  of the element material. Our measurements on the thermal conductivity, and cross-plane Seebeck coefficient of ErAs:InGaAs/InGaAlAs superlattice samples show that the incorporation of erbium arsenide metallic nanoparticles into the semiconductor superlattice structure provides an attractive way for the enhancement of the material thermoelectric properties. With the improvement of material properties, and the optimization of the generator

structure and packaging design, a superlattice thin-film generator with an output power density of over 1 W/cm<sup>2</sup> should be possible when working with heat source of 400 °C.

In summary, 400 element ErAs:InGaAs/InGaAlAs superlattice thin-film array generators were fabricated. An output power of over 0.7 mW was measured on an external load resistor of 100  $\Omega$  when the temperature drop across the whole device package was 30 K. Each superlattice element is 5  $\mu\text{m}$  thick and 200  $\mu\text{m} \times 200 \mu\text{m}$  in area size. With the optimization of superlattice property, generator and packaging design, an output power over 1 W/cm<sup>2</sup> should be achievable.

The authors acknowledge useful discussions with Dr. Mihai Gross. This work is supported by the Office of Naval Research Thermionic Energy Conversion Center MURI.

<sup>1</sup>G. J. Snyder, J. R. Lim, C. K. Huang, and J. P. Fleurial, *Nat. Mater.* **2**, 528 (2003).

<sup>2</sup>Z. H. Dughaish, *Physica B* **322**, 205 (2002).

<sup>3</sup>I. H. Kim, *Mater. Lett.* **43**, 221 (2000).

<sup>4</sup>D. M. Rowe, *CRC Handbook of Thermoelectronics* (CRC, New York, 1995).

<sup>5</sup>G. Zeng, J. E. Bowers, Y. Zhang, and A. Shakouri, *SiGe/Si Superlattice Power Generators*, Clemson University Press, Clemson, S.C., 2005, pp. 164–167.

<sup>6</sup>R. Venkatasubramanian, E. Siivola, T. Colpitts, and B. O'Quinn, *Nature* (London) **413**, 597 (2001).

<sup>7</sup>T. E. Humphrey and H. Linke, *Phys. Rev. Lett.* **94**, 096601-4 (2005).

<sup>8</sup>L. D. Hicks and M. S. Dresselhaus, *Phys. Rev. B* **47**, 12727 (1993).

<sup>9</sup>T. C. Harman, P. J. Taylor, M. P. Walsh, and B. E. LaForge, *Science* **297**, 2229 (2002).

<sup>10</sup>D. G. Cahill, W. K. Ford, K. E. Goodson, G. D. Mahan, A. Majumdar, H. J. Maris, R. Merlin, and S. R. Phillpot, *J. Appl. Phys.* **93**, 793 (2003).

<sup>11</sup>T. Koga, X. Sun, S. B. Cronin, and M. S. Dresselhaus, *Appl. Phys. Lett.* **73**, 2950 (1998).

<sup>12</sup>T. Koga, X. Sun, S. B. Cronin, and M. S. Dresselhaus, *Appl. Phys. Lett.* **75**, 2438 (1999).

<sup>13</sup>A. Shakouri and J. E. Bowers, *Appl. Phys. Lett.* **71**, 1234 (1997).

<sup>14</sup>M. J. Kelly, *Low-Dimensional Semiconductors: Materials, Physics, Technology, Devices* (Oxford University Press, New York, 1995).

<sup>15</sup>V. A. Markel and T. F. George, *Optics of Nanostructured Materials*, Wiley Series in Lasers and Applications (Wiley-Interscience, New York, 2000).

<sup>16</sup>T. M. Tritt, *Recent Trends in Thermoelectric Materials Research Iii* **71**, Ix–Xiv (2001).

<sup>17</sup>L. D. Hicks and M. S. Dresselhaus, *Phys. Rev. B* **47**, 16631 (1993).

<sup>18</sup>S. T. Huxtable, A. R. Abramson, C. L. Tien, A. Majumdar, C. LaBounty, X. Fan, G. Zeng, J. E. Bowers, A. Shakouri, and E. T. Croke, *Appl. Phys. Lett.* **80**, 1737 (2002).

<sup>19</sup>D. Vashaee and A. Shakouri, *Phys. Rev. Lett.* **92**, 106103/1 (2004).

<sup>20</sup>J. M. Zide, D. O. Klenov, S. Stemmer, A. C. Gossard, G. Zeng, J. E. Bowers, D. Vashaee, and A. Shakouri, *Appl. Phys. Lett.* **87**, 112102 (2005).

<sup>21</sup>G. Zeng, J. E. Bowers, Y. Zhang, A. Shakouri, J. M. Zide, A. C. Gossard, W. Kim, and A. Majumdar, in *ErAs/InGaAs Superlattice Seebeck Coefficient* (Clemson University Press, Clemson, S.C., 2005), pp. 485–488.

<sup>22</sup>D. G. Cahill, *Rev. Sci. Instrum.* **61**, 802 (1990).